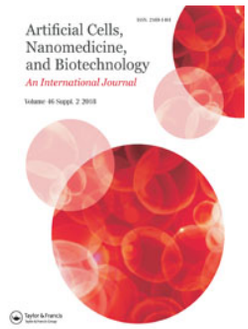

Taylor & Francis
Taylor & Francis Group

Artificial Cells, Nanomedicine, and Biotechnology

An International Journal

ISSN: 2169-1401 (Print) 2169-141X (Online) Journal homepage: https://www.tandfonline.com/loi/ianb20

Development and characterization of polymeric-based nanoparticles for sustained release of amoxicillin – an antimicrobial drug

Enes Güncüm, Nuran Işıklan, Ceren Anlaş, Nilgün Ünal, Elif Bulut & Tülay Bakırel

To cite this article: Enes Güncüm, Nuran Işıklan, Ceren Anlaş, Nilgün Ünal, Elif Bulut & Tülay Bakırel (2018) Development and characterization of polymeric-based nanoparticles for sustained release of amoxicillin – an antimicrobial drug, Artificial Cells, Nanomedicine, and Biotechnology, 46:sup2, 964-973, DOI: 10.1080/21691401.2018.1476371

To link to this article: https://doi.org/10.1080/21691401.2018.1476371

Published online: 26 May 2018.

ARTIFICIAL CELLS, NANOMEDICINE, AND BIOTECHNOLOGY
2018, VOL. 46, NO. S2, S964–S973
https://doi.org/10.1080/21691401.2018.1476371

Development and characterization of polymeric-based nanoparticles for sustained release of amoxicillin – an antimicrobial drug

Enes Güncüm[a], Nuran Işıklan[b], Ceren Anlaş[c], Nilgün Ünal[d], Elif Bulut[d] and Tülay Bakırel[c]

[a]Department of Pharmacology and Toxicology, Faculty of Veterinary Medicine, Kırıkkale University, Kırıkkale, Turkey; [b]Department of Chemistry, Faculty of Science and Arts, Kırıkkale University, Kırıkkale, Turkey; [c]Department of Pharmacology and Toxicology, Faculty of Veterinary Medicine, Istanbul University, Istanbul, Turkey; [d]Department of Microbiology, Faculty of Veterinary Medicine, Kırıkkale University, Kırıkkale, Turkey

ABSTRACT

In this study, amoxicillin (AMO)-loaded poly(vinyl alcohol)/sodium alginate (PVA/NaAlg) nanoparticles were prepared as a polymer-based controlled release system. The physicochemical properties of the obtained nanoparticles were investigated by XRD, DSC/TGA, particle size analyses and zeta potential measurements. The average particle sizes were in the range from 336.3 ± 25.66 to 558.3 ± 31.39 nm with negative zeta potential values from −41.86 ± 0.55 to −47.3 ± 2.76 mV. The influences of PVA/NaAlg ratio, span 80 concentration, exposure time to glutaraldehyde (GA) and the drug/polymer ratio on AMO release profiles were evaluated. *In vitro* drug release studies showed a controlled and pH dependent AMO release with an initial burst effect. XRD patterns and DSC thermograms of AMO-loaded nanoparticles revealed that the drug in the nanoparticles was in amorphous form, which was more stable than the crystalline form. The antibacterial activity of the optimal formulation was also investigated. The minimum inhibitory concentration (MIC) values of this formulation had the comparable antibacterial activity with that of pure AMO. These results indicate that the developed nanoparticles could be a promising candidate drug delivery system for AMO.

ARTICLE HISTORY
Revised 7 May 2018

KEYWORDS
Amoxicillin; polymeric nanocarrier; sustained release; oral drug delivery

Introduction

The use of nanotechnology to design and create a delivery system that improves the efficacy of API (Active Pharmaceutical Ingredients) stand in the foreground of today's medical science and is the key to health improvement. In this context, to achieve a suitable timed-controlled drug release resulting in steady-state plasma concentration over a long-time period, some new and interesting drug delivery systems have been developed which aim at targeting specific cell types or tissues. It has been also proved that many novel carrier systems have improved pharmacokinetic and pharmacodynamic properties of various drug molecules [1,2].

The aim of controlled drug delivery is to localize the pharmacological activity of the drug to the targeted site at desired release rates. Compared to conventional dosage forms such delivery systems present many advantages, which include enhanced efficacy, reduced toxicity and increased patient convenience and compliance [3]. While these advantages can be significant, the possible disadvantages cannot be ignored, such as non-biocompatibility or toxicity of the materials used and undesirable by-products of degradation [4]. Controlled release supported by biodegradable and biocompatible nanotechnology-based carriers can possibly improve the therapeutic efficacy of drugs, minimize their systemic adverse effects, and increase patients' adherence to the regimen through decreasing the administration frequency and dose [5–7].

Polymeric nanoparticles, as drug delivery systems, have been attracting much attention in the recent years due to their potential application in medicine and pharmaceutics. These particles are stable in the gastrointestinal (GI) tract and offer a number of advantages compared to other technologies, including protecting the encapsulated drug from the pH environment, enzyme degradation and drug efflux pump [8,9]. Moreover, they could exhibit controlled release properties and enhance drug bioavailability [10]. Many polymers, which are biodegradable and biocompatible, have been utilized to prepare nanocarriers for drug delivery [11]. Among them, sodium alginate (NaAlg) broadly used in drug delivery application [12–14].

NaAlg is a natural polysaccharide which is generated by brown algae and bacteria, and has a long story of use in many biomedical applications, as well as drug delivery systems [15,16]. It is a polyanionic linear copolymer, consisted of two types of monomeric units α-L-guluronic acid and β-D-mannuronic acid residues which considered as a unique biodegradable, biocompatible, mucoadhesive and non-toxic substance [17,18]. It is known that when in contact with glutaraldehyde or calcium ions, alginate salts create a reticulated structure, and this property has been used to design sustained release systems for various drugs [19].

CONTACT Enes Güncüm egunc@hotmail.com Department of Pharmacology and Toxicology, Faculty of Veterinary Medicine, Kırıkkale University, 71450 Yahşihan, Kırıkkale, Turkey

Another biocompatible, biodegradable and non-toxic polymer is poly(vinyl alcohol) (PVA). Because of these properties and its simple chemical structure and easiness of chemical modification, it has been extensively used in many biomedical applications including burn wound dressing, artificial muscle, contact lenses, vocal cord reconstruction and in pharmaceutical fields [20–22]. However, PVA is a hydrophilic polymer [23] and especially for drug delivery applications, its weak stability in water has restricted its use in aqueous systems. In order to overcome this issue, insoluble PVA can be formulated by cross-linking, copolymerizing, grafting and blending, which need some additional and sometimes complex and time-wasting procedures [24–26]. The method of polymer blending can be regarded as a beneficial means to prepare a new polymer blend of PVA/NaAlg. To obtain crosslinked NaAlg using glutaraldehyde, the chemical reaction between the aldehyde groups of glutaraldehyde and hydroxyl groups of NaAlg can be used [27].

The objective of this study was to prepare PVA/NaAlg blend nanoparticles that contain amoxicillin (AMO) to acquire a controlled drug release profile convenient for oral administration. Throughout the world, AMO is one of the most commonly used β-lactam antibiotics and it is prescribed to treat humans and animals [28]. This drug is an excellent agent for the treatment of a wide range of bacterial infections, including urinary tract, gastrointestinal tract, skin and soft tissue, upper and lower respiratory infections. [29,30]. However, after oral administration, its short half-life (1–1.5 h) in the circulation requires frequent dosing to maintain the steady-state plasma concentration [30–32]. Because of that, it becomes important to acquire controlled or sustained drug delivery to enhance the stability or bioavailability and to target the drug to a specific site.

Materials and methods

Materials

NaAlg (sodium alginate) (medium viscosity) was obtained from Sigma-Aldrich (Louis, USA). PVA (poly(vinyl alcohol)) was purchased from Merck (Hohenbrunn, Germany). The molecular weight and degree of hydrolysis of PVA were 145,000 and greater than 98%, respectively. Amoxicillin, span 80, glutaraldehyde (25% w/w) solution, paraffin oil, and HCl (37% puriss.) were purchased from Sigma-Aldrich (Louis, USA).

Preparation of nanoparticles

NaAlg solution (2%, w/v) was prepared in distilled water at room temperature and PVA solution (4%, w/v) was prepared in hot distilled water (80 °C) by stirring overnight. Solution of the two polymers were mixed in different ratios and stirred to form a homogeneous solution. A known amount of AMO was added to this solution (blend of PVA/NaAlg). This polymer solution containing AMO was emulsified in paraffin oil (30 ml) containing 2% (w/w) of span 80 under continuous homogenizing using a Heidolph RZR 2021 homogenizer (Heidolph Instruments, Schwabach, Germany) for 30 min at 2000 rpm. Then, a required amount of glutaraldehyde (GA) containing HCl (0.7%, v/v) was slowly dropped into this emulsion and homogenizing was continued for an additional 1 h. The nanoparticle suspension was centrifuged at 10,000 rpm for 5 min. Thereafter, the precipitated nanoparticles were washed with petroleum ether, n-hexane and ethanol to remove residual GA and paraffin oil. Finally, the obtained nanoparticles were dried in an oven at 40 °C. NaAlg nanoparticles were prepared in a similar way. Figure 1 illustrates the process of preparation of AMO-loaded nanoparticles.

Measurement of particle size and zeta potential

The mean particles size and zeta potential were determined by zetasizer (Malvern Instruments, UK). Briefly, 1 mg of the dried nanoparticles were suspended in 1.5 ml of ethanol and sonicated during 1 min to form a uniform dispersion of nanoparticles. The measurements were performed at a scattering angle of 90° at a temperature of 25 °C. Using the same procedures, zeta potential and particle size measurements were

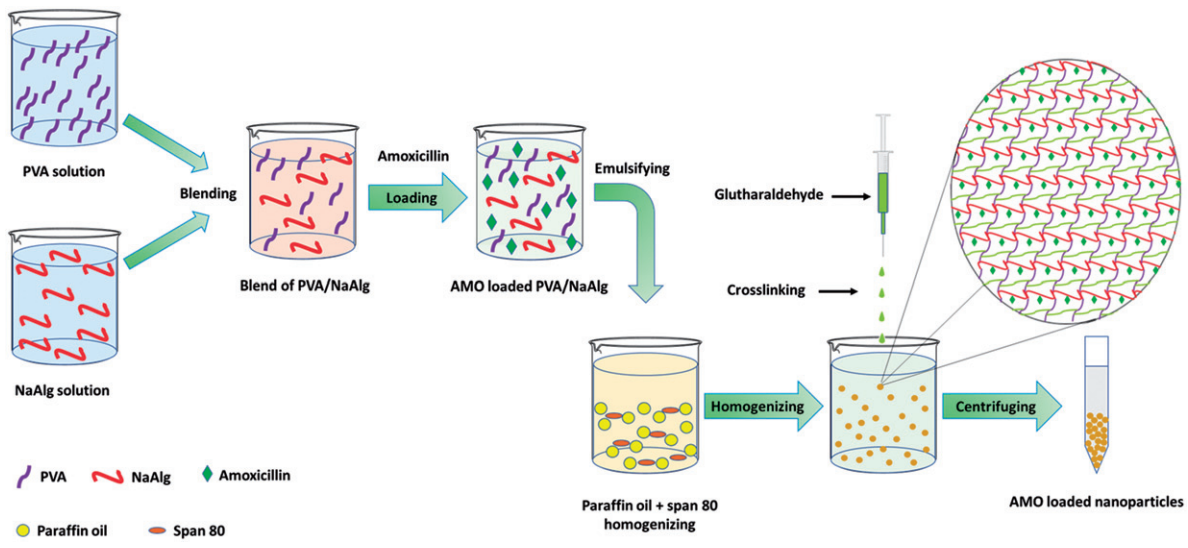

Figure 1. Schematic diagram of the preparation of AMO-loaded nanoparticles.

also performed at pH 1.2 and pH 6.8. For each sample, the measurements were repeated three times.

Determination of the drug content

A known amount of particles (10 mg) was placed in a flask and suspended in 50 ml of distilled water. The suspension was extracted at room temperature for 4 h to allow the complete extraction of AMO from the particles. After 4 h, the suspension was filtered through a filter paper and the filtrate solution was collected. The content of AMO was measured using ultraviolet-visible spectrophotometer at a wavelength of 230 nm with distilled water as a blank. The encapsulation efficiency (EE) and loading capacity (LC) were calculated according to the following equations:

$$\text{EE } (\%) = \text{Drug content in particles/Drug amount used} \times 100$$

$$\text{LC } (\%) = \text{Weight of drug in particles/Weight of particles} \times 100$$

In vitro *drug release experiments*

The *in vitro* release studies of AMO-loaded nanoparticles were carried out in 100 ml conical flasks containing 50 ml of HCl solution (pH 2.0) and 50 ml of phosphate buffer solution (pH 6.0). The flasks were incubated in a shaking water bath (100 rpm) (BS-21, Jeio Tech Co, Korea) maintained at 41 °C. Firstly, the release medium for AMO was kept at pH 2.0 (HCI solution) for 1 h. From 1 h onwards, the medium was changed to phosphate buffer solution (pH 6.0). Samples of 400 µl were withdrawn at regular time intervals over a 24-h period and the same volume of fresh HCI solution (pH 2.0) and phosphate buffer solution (pH 6.0) were replaced in the release medium to maintain constant volume. The amount of released AMO was determined by UV spectrophotometer (Perkin-Elmer) at 230 nm, and the cumulative release profile versus time was plotted. All experiments were performed in triplicate and the results were expressed as mean value and standard deviation (±SD).

Differential scanning calorimetry (DSC)

Differential scanning calorimetry was performed using DSC Q2000 instrument (TA Instruments, USA). Approximately, 2 mg of each sample was accurately weighed in aluminium pans and hermetically sealed. The DSC runs were conducted from 30 °C to 400 °C at a heating constant rate of 10 °C/min under constant purging of nitrogen at 50 ml/min.

Thermo gravimetric analysis (TGA)

In order to determine thermal stability of the samples, thermogravimetric analysis was carried out using TGA-Q500 thermogravimetric analyser (TA Instruments, USA). Samples weighing 2 mg were heated at a fixed heating rate of 10 °C/min from 30 °C to 900 °C under a nitrogen purge (50 ml/min). The loss of weight as a function of temperature was recorded.

Scanning electron microscopy (SEM)

SEM image of particles was obtained using a JEOL JSM-5600 (Japan) scanning electron microscope with an operating voltage of 20 kV. The sample was mounted on a copper stub using carbon tape and sputter-coated with a thin layer of gold in a vacuum chamber before observed under SEM.

X-ray diffractions (XRD)

The XRD patterns of AMO, AMO loaded nanoparticles and blank nanoparticles were obtained using an X-ray powder diffractometer (Rigaku Ultimate IV Diffractometer, Japan). The dried nanoparticles were mounted on sample holder, and the patterns were recorded in the range of 2–50° at the speed of 1°/min.

In vitro *antibacterial activity of the nanoparticles*

Antibacterial evaluation of the drug-loaded nanoparticle suspension (pH 6.0) and pure AMO were performed against *Escherichia coli* (ATCC 29213) and *Staphylococcus aureus* (ATCC 25922). The minimum inhibitory concentration (MIC) was determined in 96-well plates by the standard broth microdilution method according to the Clinical and Laboratory Standards Institute (CLSI) guidelines recommendations, using cation-adjusted Mueller-Hinton broth (CAMHB).

A fresh, pure culture should be used for the preparation of the bacterial inoculum. Bacteria were inoculated on Mueller-Hinton agar and incubated overnight at 37 °C. Bacterial colonies were diluted with fresh Mueller-Hinton broth to obtain optical densities corresponding to 0.5 McFarland standard. Two-fold serial dilutions of the nanoparticles and pure drug were prepared in U-bottom 96-well plates with CAMHB to achieve final concentrations ranging from 0.25 to 512 µg/ml. Then, the bacterial strains were added to each 96-well plate to give a final concentration of 5×10^5 CFU/ml. The MIC was described as the lowest concentration of the drug-loaded nanoparticles and pure AMO that completely inhibited visual growth of the bacteria after incubation at 37 °C for 24 h.

Results and discussion

Particle size, zeta potential and encapsulation efficiency

The formulation parameters, particle size, zeta potential and encapsulation efficiency of amoxicillin loaded nanoparticles are presented in Table 1. The mean diameter of particles ranged from 336.3 ± 25.66 to 558.3 ± 31.39 nm depending on the different parameters. When the particle size is examined in terms of NaAlg amount in formulations, it was found that amount of NaAlg influenced the particles size and enhancement of alginate concentration leads to increase of particle size. On the other hand, it was found that increment of encapsulation efficiency was gradually increased with the increase of NaAlg ratio in the blend formulations. In these formulations (F1, F2, F3 and F4), with a 4-fold increase in the amount of NaAlg resulted in an increase of 66.45% in encapsulation efficiency. Moreover, it was determined that the

highest encapsulation efficiency was obtained from pure NaAlg nanoparticles among all the formulations. Conversely, a negative correlation was found between the percentage of particle yields and amount of NaAlg. Considering data of particle yields and encapsulation efficiency of prepared formulations, the formulation that has maximum yield was used for further studies.

Amount of span 80 was another parameter that affects particles size. According to this, it was observed that increasing concentration of span 80 from 1% to 4% caused the decrease of particles size from 558.3 ± 31.39 to 397 ± 22.73 nm. Similarly, Jose et al. [33] and Aydogan et al. [34] have reported that higher span 80 concentration caused the smaller particle size when they prepared diltiazem-loaded microspheres and pregabalin-loaded microspheres, respectively. Relatedly, Huang et al. [35] reported that this surfactant agent (span 80) diminished particle size by reducing surface tension between liquid paraffin and organic phase in 5-fluorouracil-loaded microparticles. In fact, span 80 tends to reduce surface tension between the two phases, thereby preventing coalescence of particles by forming a thin layer around the droplets while stabilizing the emulsion. When the amount of span 80 in formulation falls below a certain concentration, droplets tend to aggregate because of insufficiency of surface tension reducing effect of surfactant agent and thus particle size is increased [33–36]. Figure 2 shows SEM microphotograph of AMO-loaded nanoparticles. From this microphotograph, it can be seen that the nanoparticles have a uniform spherical morphology.

As can be seen from Table 1, there was not any considerable difference within the zeta potentials of the nanoparticles. The average zeta potential values obtained for all the formulations were negative and observed in the range of −41.86 ± 0.55 to −47.3 ± 2.76 mV. Positive or negative surface charge can exhibit variability depending on the composition of the polymer or material used. It is thought that the negative surface charge of the particles is probably originated from negative carboxyl groups of alginate [37]. Likewise, Patil and Devarajan [38] also attributed negative surface charge of the prepared insulin-loaded alginate nanoparticles to the carboxyl groups in the polymer. The surface charge of nanoparticles with less than −30 mV or greater than 30 mV are related to the lower aggregation tendency of particles and higher stability in suspension [39,40].

The effect of different pH mediums on the particles size and zeta potential was also investigated. Table 2 shows the variations in particles size and zeta potential in different pH values (at pH 1.2 and at pH 6.8). In general, it can be seen from the table that the mean particle size of the formulations is smaller at pH 1.2 than at pH 6.8. Concomitant with alteration of PVA/NaAlg ratio from 1/1 to 1/4 at pH 1.2, it was

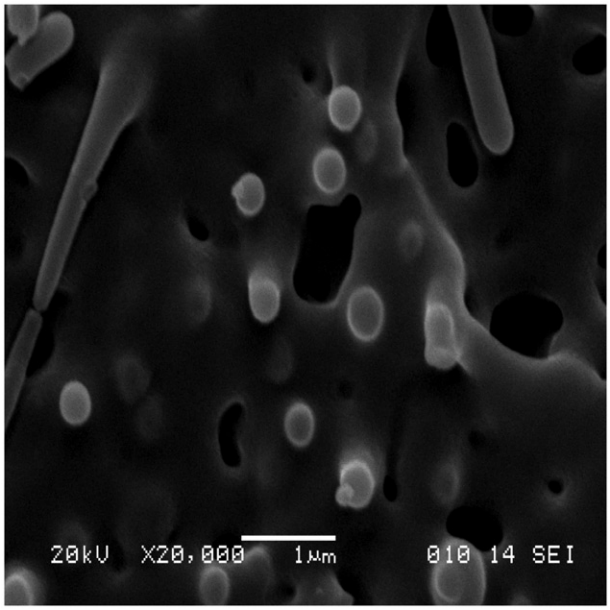

Figure 2. SEM image of AMO-loaded nanoparticles.

Table 1. Preparation condition, encapsulation efficiency (EE), particle yields, average size, and zeta potential for all formulations.

Code	Polymer	Ratio of drug/polymer (w/w)	Span 80 (%)	Exposure time to GA (h)	EE (%)	Particle yield (%)	LC (%)	Average size (nm)	Zeta potential (mV)
F1	PVA/NaAlg 1/1 (w/w)	1/2	2	1	26.74 ± 2.66	77.14 ± 4.22	12.68 ± 0.19	336.30 ± 25.66	−41.86 ± 0.55
F2	PVA/NaAlg 1/2 (w/w)	1/2	2	1	30.42 ± 1.52	75.47 ± 0.37	12.70 ± 0.47	415.40 ± 28.32	−43.40 ± 1.95
F3	PVA/NaAlg 1/3 (w/w)	1/2	2	1	38.95 ± 1.91	71.99 ± 5.30	12.76 ± 0.80	452.50 ± 35.82	−44.20 ± 1.22
F4	PVA/NaAlg 1/4 (w/w)	1/2	2	1	44.51 ± 4.17	71.03 ± 5.55	13.99 ± 0.26	502.72 ± 15.92	−45.12 ± 1.10
F5	NaAlg	1/2	2	1	62.65 ± 0.95	47.33 ± 1.52	22.75 ± 0.75	527.00 ± 14.66	−47.30 ± 2.76
F6	PVA/NaAlg 1/4 (w/w)	1/2	2	0.5	33.85 ± 0.98	67.22 ± 5.80	11.27 ± 0.50	449.40 ± 14.70	−42.50 ± 1.12
F7	PVA/NaAlg 1/4 (w/w)	1/2	2	2	36.46 ± 3.09	67.84 ± 1.50	13.61 ± 0.63	374.30 ± 15.16	−44.00 ± 1.95
F8	PVA/NaAlg 1/4 (w/w)	1/2	1	1	33.15 ± 2.02	79.23 ± 0.86	12.04 ± 0.97	558.30 ± 31.39	−44.50 ± 3.82
F9	PVA/NaAlg 1/4 (w/w)	1/2	4	1	33.53 ± 1.06	73.11 ± 5.67	11.27 ± 0.66	397.00 ± 22.73	−45.50 ± 4.52
F10	PVA/NaAlg 1/4 (w/w)	1/1	2	1	35.79 ± 1.34	59.57 ± 2.89	17.89 ± 0.96	465.60 ± 23.85	−44.80 ± 1.37
F11	PVA/NaAlg 1/4 (w/w)	1/4	2	1	40.63 ± 1.12	73.73 ± 2.05	8.12 ± 0.20	436.90 ± 20.93	−41.90 ± 2.91

Data were presented as the mean ± SD ($n = 3$).

observed that the particles size decreased. The particle size of the formulation with PVA/NaAlg ratio 1/1 (F1) was 304.20 ± 22.05 nm and particle size decreased to 213.51 ± 17.64 nm with 4-fold increasing NaAlg ratio (F4). The least particle size was obtained from pure NaAlg nanoparticles (F5) with 130.51 ± 16.95 nm. On the contrary, at pH 6.8, it was found that with the changing of PVA/NaAlg from 1/1 to 1/4, the particles size increased from 366.40 ± 26.64 nm to 512.00 ± 7.49 nm. It was reported that NaAlg has the property of shrinking at low pH and the obtained data could be associated with the fact that because the pK_a of NaAlg is about 3.2, most of $-COO^-$ groups in NaAlg converted into $-COOH$ groups in low pH. In NaAlg, the hydrogen bonding between $-COOH$ groups leads to the polymer–polymer interactions and predominates over the polymer–water interactions. Resulted from this, the particle size of the formulations is relatively small at pH 1.2. When the pH is increased, the $-COOH$ groups of NaAlg molecules tend to ionize and give $-COO^-$ ions that facilitate the swelling of the formulations [20,41]. Hence, the particles size increased at pH 6.8.

On the other hand, at both pH, the zeta potential of the obtained formulations showed negative values. Generally speaking, compared to at pH 1.2, the formulations had more negative zeta potential values at pH 6.8. This behaviour can be explained as the result of protonation of the carboxyl groups (−COOH) on the NaAlg molecules when the pH decreased below their pK_a value [42]. Here too, it was found that the obtained data were influenced by PVA/NaAlg ratio in the formulation. An increase in the amount of NaAlg enhanced the negative values of the formulations (F1, F2, F3 and F4) and the values reached from −2.13 ± 0.75 mV to −6.03 ± 1.90 mV at pH 1.2 and from −21.70 ± 1.83 mV to −33.60 ± 1.17 mV at pH 6.8, respectively. The most negative zeta potential values were recorded for pure NaAlg nanoparticles (F5).

Table 2. The effect of different pH on particles size and zeta potential.

	Average size (nm)		Zeta potential (mV)	
Formulation code	pH 1.2	pH 6.8	pH 1.2	pH 6.8
F1	304.20 ± 22.05	366.40 ± 26.64	−2.13 ± 0.75	−21.70 ± 1.83
F2	249.86 ± 6.72	497.20 ± 3.58	−4.70 ± 2.59	−30.63 ± 0.25
F3	236.40 ± 22.00	503.46 ± 1.92	−5.64 ± 0.90	−32.90 ± 1.30
F4	213.51 ± 17.64	512.00 ± 7.49	−6.03 ± 1.90	−33.60 ± 1.17
F5	130.51 ± 16.95	576.60 ± 8.12	−8.39 ± 1.14	−36.95 ± 1.76
F6	194.87 ± 3.66	552.73 ± 4.77	−6.09 ± 1.96	−33.16 ± 1.59
F7	238.53 ± 23.37	501.93 ± 6.90	−5.75 ± 1.48	−34.10 ± 1.56
F8	229.10 ± 23.05	590.33 ± 15.61	−1.61 ± 1.24	−30.46 ± 0.84
F9	199.18 ± 7.11	559.60 ± 7.37	−6.76 ± 2.19	−25.96 ± 2.23
F10	233.40 ± 24.31	515.13 ± 0.75	−2.48 ± 2.25	−33.03 ± 1.88
F11	220.68 ± 21.17	612.46 ± 13.01	−6.01 ± 2.17	−33.23 ± 1.15

Data were presented as the mean ± SD ($n = 3$).

In vitro *drug release*

In vitro release of AMO from particles were carried out in pH 2.0 (HCl solution) and pH 6.0 (phosphate buffer solution). As shown in Figures 3–6, in all formulations the drug release from particles proceeded in two stages: an initial rapid release approximately in the first 1.5 h followed by a slower sustained release up to 24 h. The initial rapid release could be owing to the burst release of drug from the particles. A possible explanation of this situation could be that the faster migration of the weakly localized or bound drug molecules on the surface of particles. The subsequent slow release is likely due to slower migration of the remaining drug entrapped in the inner region of the particles [43,44].

The release results were evaluated in terms of parameters such as drug/polymer ratio, PVA/NaAlg ratio, crosslinking time and amount of surfactant agent. Cumulative release results of AMO are presented in Figure 3 depending on the different PVA/NaAlg ratio in the formulations. Accordingly, the drug release rate increased with increment of NaAlg in the formulations. Among PVA/NaAlg blend formulations (F1, F2, F3 and F4) the highest release rate was obtained from F4 formulation with 51.11%, while the lowest release rate was obtained from F1 formulation with 41.50%. On the other side, the maximum release rate was found in NaAlg nanoparticles with 54.90%. As similar result was reported by Şanlı et al.

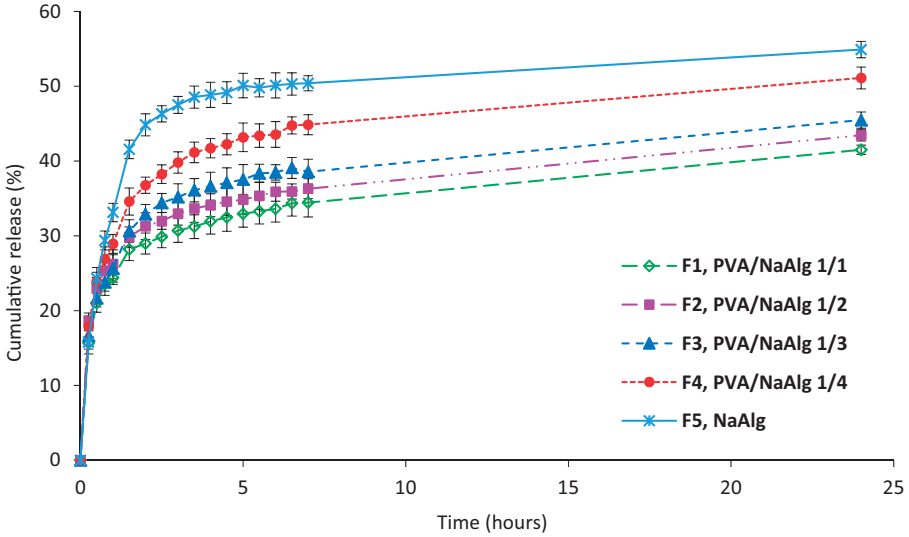

Figure 3. Effect of the ratio of PVA/NaAlg on AMO release (concentration of span 80 = 2%, exposure time to GA = 1 h, ratio of drug/polymer = 1/2). Data were presented as the mean ± SD ($n = 3$).

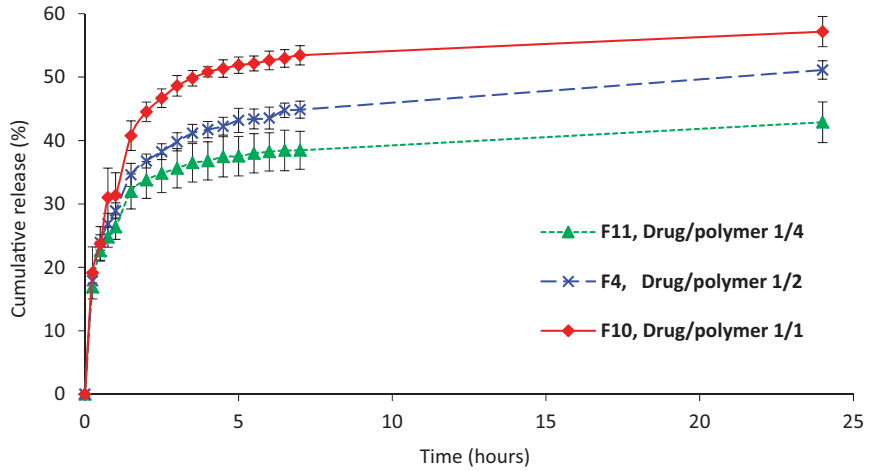

Figure 4. Effect of the ratio of drug/polymer on AMO release (concentration of span 80 = 2%, exposure time to GA = 1 h, ratio of PVA/NaAlg = 1/4). Data were presented as the mean ± SD ($n = 3$).

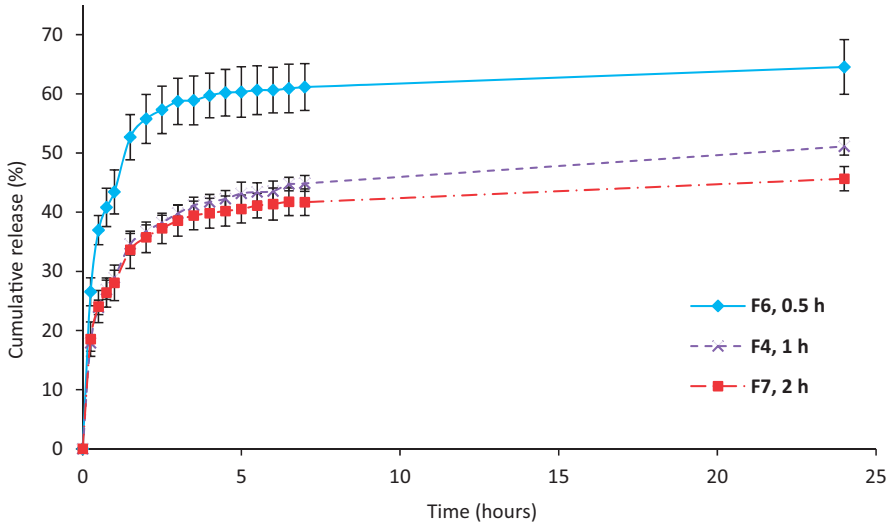

Figure 5. Effect of the exposure time to GA on AMO release (concentration of span 80 = 2%, ratio of drug/polymer = 1/2, ratio of PVA/NaAlg = 1/4). Data were presented as the mean ± SD ($n = 3$).

[25], it is thought that release rate differences are caused by NaAlg containing hydroxyl and carboxyl groups that provide hydrophilicity to the molecule. Compared to NaAlg, PVA has a small hydrated volume and therefore PVA creates an intensive network of macromolecular chains in the blend formulations. So, in comparison with NaAlg, permeation of liquid molecules by means of PVA/NaAlg blend formulations and afterwards diffusion of the drug to the external medium becomes more difficult [45,46].

The drug/polymer ratio in the formulations was investigated as one of the parameters that affect the release profile. According to the release results (Figure 4), it was found that the release rate of the formulation with the highest drug/polymer ratio was higher than the other formulations. Accordingly, in the formulation that the drug/polymer ratio is equal (F10), the highest release rate was achieved with 57.16%, whereas when the ratio is reduced by 1/4, the release rate decreased to 42.88%. It is considered that this is probably related to the presence of more free void spaces, through that, a fewer amount of drug molecules will carry. Similarly, Babu et al. [19], in nifedipine loaded NaAlg-MC (methyl cellulose) blend formulations and Swamy et al. [47], in triprolidine loaded poly (hydroxy ethyl methyl acrylate-co-acrylic acid) carrier system, reported that the release levels were increased depending on the increased amount of drugs.

The exposure time to cross-linking agent (GA) was another parameter affecting the release profile. As shown in Figure 5, there is a negative correlation between the cross-linking time and the release rate. When the exposure time to GA was increased from 0.5 h to 2 h, the release rate decreased from 64.54% to 45.65%. The measured decline in the release rate is presumably because of the increasing cross-linking time that enhances the cross-link density of the particles, which support compact network of the polymer. As a result, the free space of the matrix reduces due to the high cross-link density and thus passage of drug molecules becomes difficult through the matrix [48].

The effect of different concentration of span 80 in the particles on the release profile was also investigated. Figure 6 illustrates that when the amount of span 80 increased the rate of drug release from the particles was increased. Berkland et al. [49] linked the increase in drug release rate

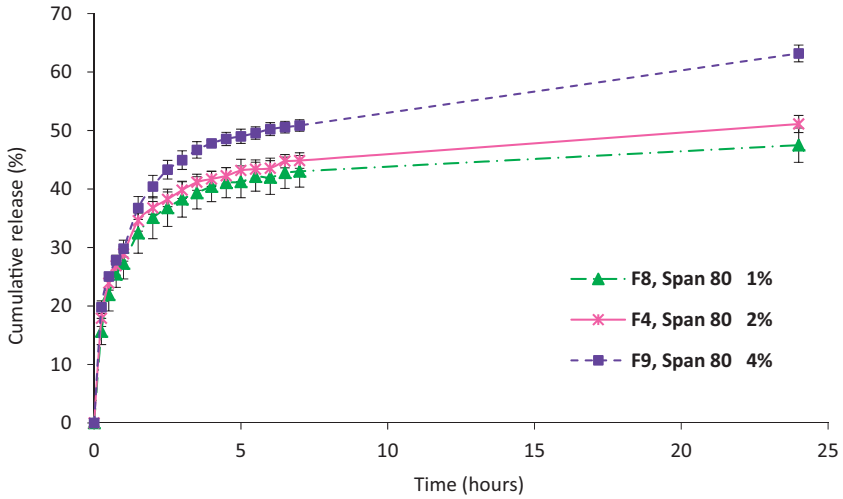

Figure 6. Effect of concentration of span 80 on AMO release (exposure time to GA =1 h, ratio of drug/polymer =1/2, ratio of PVA/NaAlg =1/4). Data were presented as the mean ± SD ($n = 3$).

Table 3. Release kinetics parameters of AMO from different formulations.

	pH of medium 2.0			pH of medium 6.0		
Formulation code	Release exponent (n)	Regression coefficient (r)	Kinetic constant (k)	Release exponent (n)	Regression coefficient (r)	Kinetic constant (k)
F1	0.32	0.964	1.403	0.14	0.996	1.420
F2	0.25	0.980	1.428	0.13	0.995	1.452
F3	0.31	0.985	1.415	0.13	0.976	1.478
F4	0.33	0.983	1.486	0.13	0.963	1.540
F5	0.53	0.991	1.531	0.11	0.910	1.615
F6	0.35	0.965	1.652	0.09	0.917	1.715
F7	0.30	0.980	1.457	0.10	0.919	1.529
F8	0.40	0.984	1.448	0.13	0.911	1.513
F9	0.29	0.993	1.479	0.18	0.966	1.557
F10	0.38	0.954	1.510	0.16	0.942	1.599
F11	0.32	0.972	1.432	0.10	0.965	1.500

from microspheres to the high surface-to-volume ratio due to decrease in particles size. As mentioned above, in our study, the increase in amount of span 80 in the formulation reduced the size of the particles. In that case, it can be said that the decrease of particles size might have been contributed to the faster release rate due to the increased surface-to-volume ratio. These data show that it is possible to achieve desired particle size and release rate with changing amount of surfactant agent.

Drug release kinetics

In order to explain the release mechanism of AMO from particles, the obtained results were fitted using the Korsmeyer–Peppas model [50].

$$\frac{Mt}{M\infty} = \mathrm{kt}^{\mathrm{n}}$$

where $Mt/M\infty$ represents the fraction of AMO released at time t, k is a kinetic constant, and the exponent n has been suggested as indicative of the release mechanism. The n value is related to the drug release mechanism. Within this context, $n \leq 0.43$ indicates Fickian diffusion, $n = 0.85$ means Case II transport (zero order), and $0.43 < n < 0.85$ indicates an anomalous behaviour (non-Fickian diffusion) [50]. The calculated values of n, k and regression coefficient (r) for all formulations are given in Table 3. As can be seen from the table, the values of n for all formulations were found to be less than 0.43 at pH 2.0 and 6.0 except for F5 (NaAlg). These obtained values of n from *in vitro* AMO release revealed that the mechanism of release is Fickian diffusion, means that AMO release from nanocarriers is mainly governed by the drug diffusion. On the other hand, the calculated n value of F5 ($0.43 < n < 0.85$ at pH 2.0) indicated that anomalous (non-Fickian diffusion: means a coupling of diffusion and polymer relaxation) was the main release mechanism for this formulation.

XRD, DSC and TGA analyses

The DSC thermogram of AMO, blank nanoparticles and drug-loaded nanoparticles obtained under nitrogen atmosphere are displayed in Figure 7. In DSC thermogram of AMO, an endothermic peak was observed at 104 °C corresponding to its melting point. The DSC curve of blank nanoparticles showed a weak endothermic peak at 201 °C. However, it can be seen from the DSC thermogram that AMO-loaded nanoparticles did not exhibit an endothermic peak at 104 °C; instead a weak endothermic peak emerged at 208 °C. The disappearance of the melting endothermic peak of AMO demonstrates that crystalline form of AMO might have been converted into amorphous form or molecularly dispersed into the polymeric matrix during the preparation of

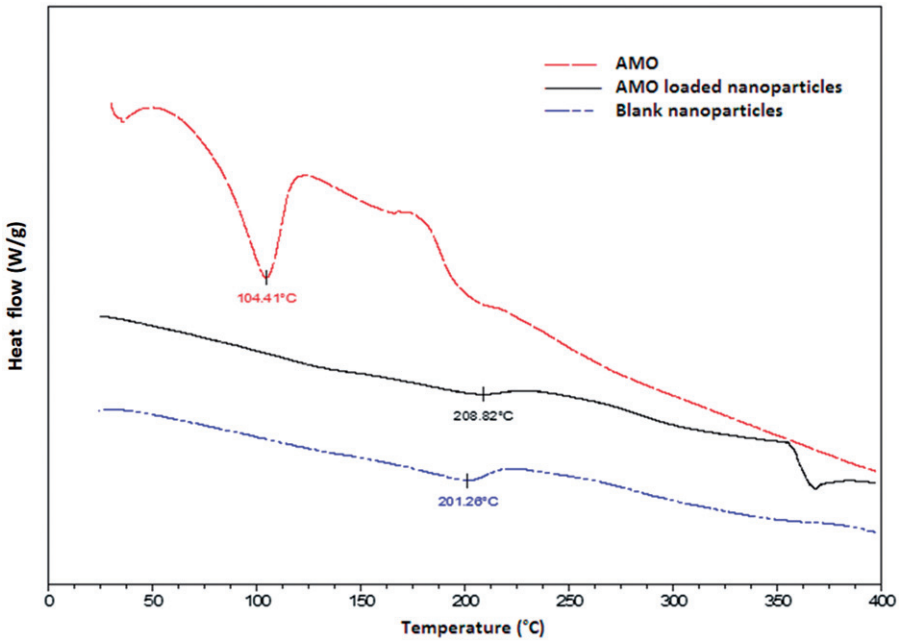

Figure 7. DSC thermograms of amoxicillin (AMO) blank nanoparticles and AMO loaded nanoparticles

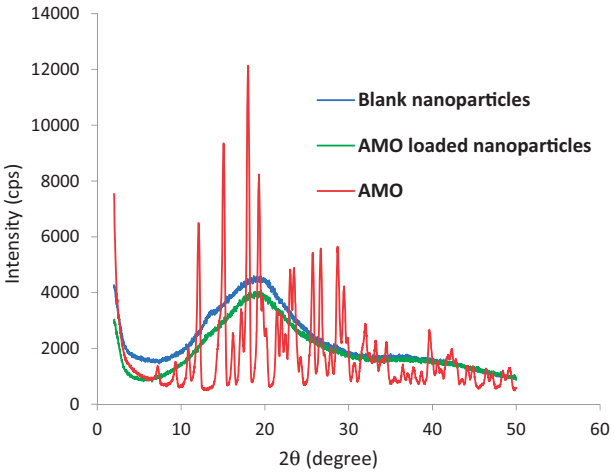

Figure 8. XRD diagrams of AMO, blank nanoparticles and AMO loaded nanoparticles.

nanoparticles [51,52]. This result was further confirmed by XRD analysis. The XRD diffractograms of AMO, blank nanoparticles and drug-loaded nanoparticles are presented in Figure 8. The intense peaks of AMO were observed at 2θ of 12°, 15°, 18°, 19°, 23.5°, 26.6° and 28.6° inferring its crystalline structure. However, the characteristic peaks of the drug were not observed in drug-loaded nanoparticles. The absence of characteristic peaks of AMO in drug-loaded nanoparticles along with the existence of halo pattern spectrum could be attributed that AMO in the nanoparticles was in amorphous form [53]. It is reported that, because of its much more saturation solubility, amorphous form of drug is a desirable characteristic of a drug in nanoparticles compared to crystalline form. This leads to a higher shelf life and long-term stability of drug in aqueous suspensions by preventing the phenomenon of Ostwald ripening in such systems [53,54].

The TGA curves of AMO, blank nanoparticles and drug-loaded nanoparticles are given in Figure 9. The first thermal degradation and weight loss of AMO were observed around 100 °C and about 12.5%, respectively, which were probably due to the water evaporation. The second thermal event was around 200 °C and it could be related to the decomposition of AMO. The temperature at which 50% weight loss of AMO occurred was around 294 °C. However, in the event of the drug-loaded nanoparticles, the temperature at which 50% weight loss occurred was found at higher temperature (around 367 °C) when compared to the pure drug. These results obviously reveal that owing to encapsulation of the drug between polymeric chains, the stability of the drug is increased [55]. From the TGA curves, it also can be seen that the stability of drug loaded nanoparticles is relatively higher than that of pure AMO.

In vitro *antibacterial activity of the nanoparticles*

The MICs of pure AMO and amoxicillin loaded nanoparticles against *E. coli* and *S. aureus* are shown in Table 4. In our study, the MIC values of pure AMO were found to be 8 μg/ml for *E. coli* and 4 μg/ml for *S. aureus*. On the other side, when the drug was loaded into nanoparticles, these MIC values were found to be 16 μg/ml and 4 μg/ml, respectively. From these results, for *S. aureus*, it can be said that there was not much change regarding the antibacterial activity of amoxicillin nanoparticles in *in vitro* conditions, was comparable with pure AMO and was not affected due to encapsulation with nanoparticles [56]. However, for *E. coli*, the antibacterial activity of the nanoparticles was found to be less effective than pure AMO. This situation can be explained by the structural difference of the cell wall of *S. aureus* (Gram positive) and *E. coli* (Gram negative) [57].

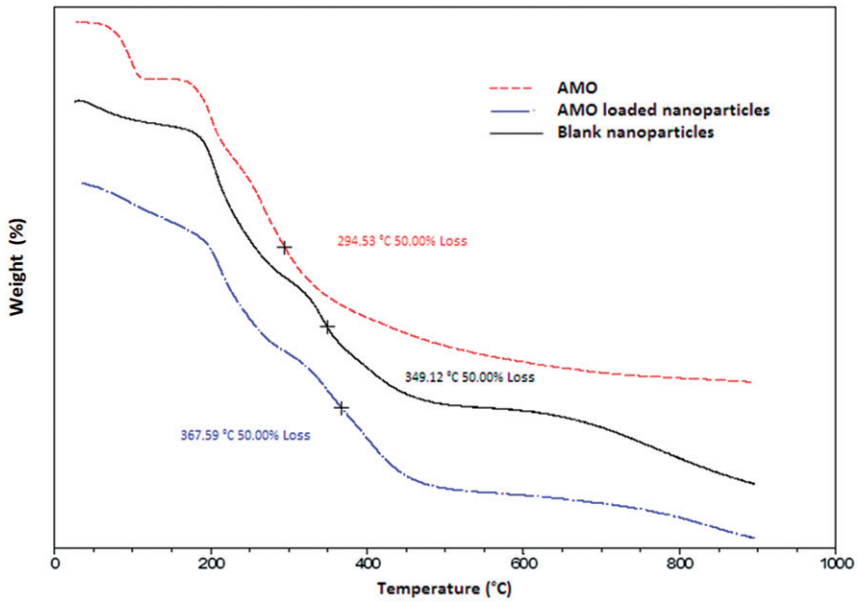

Figure 9. TGA diagrams of amoxicillin (AMO), blank nanoparticle and AMO-loaded nanoparticles.

Table 4. Minimum inhibitory concentration of AMO and AMO loaded nanoparticles (F4) against *E. coli* and *S. aureus*.

	MIC (μg/ml)	
Sample	*E. coli*	*S. aureus*
AMO	8	4
AMO-loaded nanoparticles (F4)	16	4

Conclusion

In the current study, blend nanoparticles of PVA/NaAlg with AMO loading were prepared and characterized with respect to their particle size, zeta potential, encapsulation efficiency and *in vitro* release studies. The obtained nanoparticles have a negative surface charge and enhanced stability. The release profiles of these nanoparticles were investigated under different pH conditions. Release data showed that, after an initial burst release of the drug, release rate decreased with an increase of pH and followed by a controlled release phase. The MIC value of optimal formulation toward *E. coli* and *S. aureus* was comparable with that of pure AMO. Encapsulation of AMO in PVA/NaAlg nanoparticles did not invalidate its antibacterial activity. These results reveal that the prepared PVA/NaAlg nanoparticles could be used as a useful carrier for the sustained release of AMO.

Disclosure statement

No potential conflict of interest was reported by the authors.

Funding

This work was supported by Department of Scientific Research Projects, Istanbul University [Project number: 44188].

References

[1] Demirbag B, Kardesler S, Buyuksungur A, et al. Nanotechnology in biomaterials: Nanoparticulates as drug delivery systems. In: Reisner DE, editor. Bionanotechnology II: Global prospects. Boca Raton (FL): CRC Press; 2011. p. 227–246.
[2] Lühder F, Reichardt HM. Novel drug delivery systems tailored for improved administration of glucocorticoids. Int J Mol Sci. 2017;18:1836.
[3] Singh M, Hemant K, Ram M, et al. Microencapsulation: a promising technique for controlled drug delivery. Res Pharm Sci. 2010;5:65–77.
[4] Bhowmik D, Gopinath H, Kumar BP, et al. Controlled release drug delivery systems. The Pharma Innovation. 2012;1:24–32.
[5] Lee JH, Yeo Y. Controlled drug release from pharmaceutical nanocarriers. Chem Eng Sci. 2015;125:75–84.
[6] Lee J. Nanoparticle-assisted controlled drug release. J Nanomedine Biotherapeutic Discov. 2014;4:1–2.
[7] Sanjay ST, Dou M, Fu G, et al. Controlled drug delivery using microdevices. Curr Pharm Biotechnol. 2016;17:772–787.
[8] Kumar GV, Su CH, Velusamy P. Ciprofloxacin loaded genipin cross-linked chitosan/heparin nanoparticles for drug delivery application. Materials Lett. 2016;180:119–122.
[9] Hu Y, Jiang XQ, Ding Y, et al. Preparation and drug release behaviors of nimodipine-loaded poly(caprolactone)-poly(ethylene oxide)-polylactide amphiphilic copolymer nanoparticles. Biomaterials. 2003;24:2395–2404.
[10] Pandey R, Ahmad Z, Sharma S, et al. Nano-encapsulation of azole antifungals: potential applications to improve oral drug delivery. Int J Pharm. 2005;301:268–276.
[11] Liu Z, Jiao Y, Wang Y, et al. Polysaccharides-based nanoparticles as drug delivery systems. Adv Drug Deliv Rev. 2008;60:1650–1662.
[12] Katuwavila NP, Perera ADLC, Dahanayake D, et al. Alginate nanoparticles protect ferrous from oxidation: potential iron delivery system. Int J Pharmaceut. 2016;513:404–409.
[13] Paques JP, van der Linden E, van Rijn CJM, et al. Preparation methods of alginate nanoparticles. Adv Colloid Interface Sci. 2014;209:163–171.
[14] Rastogi R, Sultana Y, Aqil M, et al. Alginate microspheres of isoniazid for oral sustained drug delivery. Int J Pharm. 2007;334:71–77.
[15] Machado AHE, Lundberg D, Ribeiro AJ, et al. Preparation of calcium alginate nanoparticles using water-in-oil (w/o) nanoemulsions. Langmuir. 2012;28:4131–4141.
[16] Motwani SK, Chopra S, Talegaonkar S, et al. Chitosan-sodium alginate nanoparticles as submicroscopic reservoirs for ocular delivery: formulation, optimisation and in vitro characterisation. Eur J Pharm Biopharm. 2008;68:513–525.
[17] Lertsutthiwong P, Noomun K, Jongaroonngamsang N, et al. Preparation of alginate nanocapsules containing turmeric oil. Carbohyd Polym. 2008;74:209–214.

[18] Kanokpanont S, Rungnapha Y, Pornanong A. Stability enhancement of mulberry-extracted anthocyanin using alginate/chitosan microencapsulation for food supplement application. Artif Cells Nanomed Biotechnol. 2018;46:773–782.
[19] Ramesh Babu V, Sairam M, Hosamani KM, et al. Preparation of sodium alginate–methylcellulose blend microspheres for controlled release of nifedipine. Carbohyd Polym. 2007;69:241–250.
[20] Hua S, Ma H, Li X, et al. pH-sensitive sodium alginate/poly(vinyl alcohol) hydrogel beads prepared by combined Ca2+ crosslinking and freeze-thawing cycles for controlled release of diclofenac sodium. Int J Biol Macromol. 2010;46:517–523.
[21] Islam A, Yasin T. Controlled delivery of drug from pH sensitive chitosan/poly (vinyl alcohol) blend. Carbohyd Polym. 2012;88: 1055–1060.
[22] Zheng H, Du YM, Yu JH, et al. Preparation and characterization of chitosan/poly(vinyl alcohol) blend fibers. J Appl Polym Sci. 2001;80:2558–2565.
[23] Kenawy ER, Abdel-Hay FI, El-Newehy MH, et al. Controlled release of ketoprofen from electrospun poly(vinyl alcohol) nanofibers. Mat Sci Eng A-Struct. 2007;459:390–396.
[24] Jannesari M, Varshosaz J, Morshed M, et al. Composite poly(vinyl alcohol)/poly(vinyl acetate) electrospun nanofibrous mats as a novel wound dressing matrix for controlled release of drugs. Int J Nanomed. 2011;6:993–1003.
[25] Sanli O, Ay N, Isiklan N. Release characteristics of diclofenac sodium from poly(vinyl alcohol)/sodium alginate and poly(vinyl alcohol)-grafted-poly(acrylamide)/sodium alginate blend beads. Eur J Pharm Biopharm. 2007;65:204–214.
[26] Arthanari S, Mani G, Jang JH, et al. Preparation and characterization of gatifloxacin-loaded alginate/poly (vinyl alcohol) electrospun nanofibers. Artif Cells Nanomed Biotechnol. 2016;44: 847–852.
[27] Swamy BY, Prasad CV, Reddy C, et al. Preparation of sodium alginate/poly (vinyl alcohol) blend microspheres for controlled release applications. J Appl Polym Sci. 2012;125:555–561.
[28] Santos DP, Bergamini MF, Zanoni MVB. Voltammetric sensor for amoxicillin determination in human urine using polyglutamic acid/glutaraldehyde film. Sens Actuators B Chem. 2008;133: 398–403.
[29] Palanikumar L, Ramasamy S, Hariharan G, et al. Influence of particle size of nano zinc oxide on the controlled delivery of amoxicillin. Appl Nanosci. 2013;3:441–451.
[30] Patel J, Patel H, Patel N, et al. Preparation, characterization and antimicrobial activity of acrylate copolymer bound amoxycillin. Indian J Pharm Sci. 2007;69:784.
[31] Angadi SC, Manjeshwar LS, Aminabhavi TM. Novel composite blend microbeads of sodium alginate coated with chitosan for controlled release of amoxicillin. Int J Biol Macromol. 2012;51: 45–55.
[32] Yellanki SK, Singh J, Syed JA, et al. Design and characterization of amoxicillin trihydrate mucoadhesive microspheres for prolonged gastric retention. Int J Pharm Sci Drug Res. 2010;2:112–114.
[33] Jose S, Prema MT, Chacko AJ, et al. Colon specific chitosan microspheres for chronotherapy of chronic stable angina. Colloids Surf B Biointerfaces. 2011;83:277–283.
[34] Aydogan E, Comoglu T, Pehlivanoglu B, et al. Process and formulation variables of pregabalin microspheres prepared by w/o/o double emulsion solvent diffusion method and their clinical application by animal modeling studies. Drug Dev Ind Pharm. 2015;41:1311–1320.
[35] Huang Y, Wei YM, Yang HR, et al. A 5-fluorouracil-loaded floating gastroretentive hollow microsphere: development, pharmacokinetic in rabbits, and biodistribution in tumor-bearing mice. Drug Des Dev Ther. 2016;10:997–1008.
[36] Chaurasia M, Chourasia MK, Jain NK, et al. Cross-linked guar gum microspheres: a viable approach for improved delivery of anticancer drugs for the treatment of colorectal cancer. Aaps Pharmscitech. 2006;7:143–151.
[37] Rescignano N, Fortunati E, Armentano I, et al. Use of alginate, chitosan and cellulose nanocrystals as emulsion stabilizers in the synthesis of biodegradable polymeric nanoparticles. J Colloid Interf Sci. 2015;445:31–39.
[38] Patil NH, Devarajan PV. Insulin-loaded alginic acid nanoparticles for sublingual delivery. Drug Deliv. 2016;23:429–436.
[39] Woitiski CB, Neufeld RJ, Ribeiro AJ, et al. Colloidal carrier integrating biomaterials for oral insulin delivery: influence of component formulation on physicochemical and biological parameters. Acta Biomater. 2009;5:2475–2484.
[40] Guo D, Dou D, Li X, et al. Ivermection-loaded solid lipid nanoparticles: preparation, characterisation, stability and transdermal behaviour. Artif Cells Nanomed Biotechnol. 2018;46:255–262.
[41] Arora S, Budhiraja RD. Chitosan-alginate microcapsules of amoxicillin for gastric stability and mucoadhesion. J Adv Pharm Technol Res. 2012;3:68–74.
[42] Hu K, McClements DJ. Fabrication of biopolymer nanoparticles by antisolvent precipitation and electrostatic deposition: zein-alginate core/shell nanoparticles. Food Hydrocoll. 2015;44:101–108.
[43] Sun DQ, Xue AY, Zhang B, et al. Enhanced oral bioavailability of acetylpuerarin by poly(lactide-co-glycolide) nanoparticles optimized using uniform design combined with response surface methodology. Drug Des Dev Ther. 2016;10:2029–2039.
[44] Dudhipala N, Veerabrahma K. Candesartan cilexetil loaded solid lipid nanoparticles for oral delivery: characterization, pharmacokinetic and pharmacodynamic evaluation. Drug Deliv. 2016;23:395–404.
[45] Şanlı O, Solak EK. Controlled release of naproxen from sodium alginate and poly(vinyl alcohol)/sodium alginate blend beads crosslinked with glutaraldehyde. J Appl Polym Sci. 2009; 112:2057–2065.
[46] Bajpai AK, Giri A. Swelling dynamics of a macromolecular hydrophilic network and evaluation of its potential for controlled release of agrochemicals. React Funct Polym. 2002;53:125–141.
[47] Swamy BY, Prasad CV, Rao KC, et al. Preparation and characterization of poly (hydroxy ethyl methyl acrylate-co-acrylic acid) microspheres for drug delivery application. International J Polym Mater Polym Biomater. 2013;62:700–705.
[48] Xiong L, He Z. Release behavior and cytotoxicity of poly (vinyl alcohol)/chitosan blend microspheres containing 2, 4-dihydroxy-5-fluoropyrimidine. Polym Plast Technol Eng. 2012;51:729–733.
[49] Berkland C, King M, Cox A, et al. Precise control of plg microsphere size provides enhanced control of drug release rate. J Control Release. 2002;82:137–147.
[50] Stulzer HK, Tagliari MP, Parize AL, et al. Evaluation of cross-linked chitosan microparticles containing acyclovir obtained by spray-drying. Mater Sci Eng C Mater Biol Appl. 2009;29:387–392.
[51] Mandal S, Basu SK, Sa B. Ca2+ ion cross-linked interpenetrating network matrix tablets of polyacrylamide-grafted-sodium alginate and sodium alginate for sustained release of diltiazem hydrochloride. Carbohyd Polym. 2010;82:867–873.
[52] Mishra B, Padaliya R, Patel RR. Exemestane encapsulated vitamin E-TPGS–polymeric nanoparticles: preparation, optimization, characterization, and in vitro cytotoxicity assessment. Artif Cells Nanomed Biotechnol. 2017;45:522–534.
[53] Kalaria D, Sharma G, Beniwal V, et al. Design of biodegradable nanoparticles for oral delivery of doxorubicin: in vivo pharmacokinetics and toxicity studies in rats. Pharm Res. 2009;26:492–501.
[54] Bairwa K, Jachak SM. Nanoparticle formulation of 11-keto-β-boswellic acid (kba): Anti-inflammatory activity and in vivo pharmacokinetics. Pharm Biol. 2016;54:2909–2916.
[55] Sharma A, Gupta A, Rath G, et al. Electrospun composite nanofiber-based transmucosal patch for anti-diabetic drug delivery. J Mater Chem B. 2013;1:3410–3418.
[56] Maya S, Indulekha S, Sukhithasri V, et al. Efficacy of tetracycline encapsulated o-carboxymethyl chitosan nanoparticles against intracellular infections of staphylococcus aureus. Int J Biol Macromol. 2012;51:392–399.
[57] Mekkawy AI, El-Mokhtar MA, Nafady NA, et al. In vitro and in vivo evaluation of biologically synthesized silver nanoparticles for topical applications: effect of surface coating and loading into hydrogels. Int J Nanomedicine. 2017;12:759–777.